New Measurement of (G_E/G_M) for the Proton

R. E. Segel (Spokesperson)
Northwestern University, Evanstan, IL

J. Arrington (Spokesperson), F. Dohrmann, D. Gaskell,
D. F. Geesaman, K. Hafidi, R. J. Holt, H. E. Jackson,
D. H. Potterveld, P. E. Reimer, K. Wijesooriya, B. Zeidman
Argonne National Laboratory, Argonne, IL

E. Brash, O. Gayou, C. Perdrisat, V. Punjabi
College of William and Mary, Williamsburg, VA

O. K. Baker
Hampton University, Hampton, VA

R. Ent, J. Gomez, C. W. de Jager, M. Jones, J. Mitchell
Jefferson Laboratory, Newport News, VA

R. Gilman, C. Glashausser, R. Ransome
Rutgers University, New Brunswick, NJ

December 13, 2000

1 Introduction

The structure of the proton is a matter of universal interest in nuclear and particle physics. Charge and current distributions are obtained through measurements of the electric and magnetic form factors, G_E and G_M, and so it is extremely important to determine these quantities as accurately as possible. The form factors are a function of the square of the four-momentum transfer, Q^2, and can be separated out by measuring the e-p elastic scattering cross section at two values of the virtual photon polarization parameter, ϵ, i.e. by performing a Rosenbluth separation. Several such measurements have been reported [1, 2] and the results are shown in figure 1, expressing G_M in units of the magnetic moment of the proton μ_p (as is done throughout this proposal). Global fits [1, 3] to these data find that G_E/G_M = 1 to within 0.1 with no significant Q^2-dependence. While no experiment strongly disagrees with a constant value of G_E/G_M, the measurements show somewhat inconsistent trends. Procedures for radiative corrections have improved since the earlier experiments ran, but the radiative corrections were redone for the global analysis. In addition, for $Q^2 < 3.5$ GeV^2, removing any single L-T measurement from the global analysis does not significantly change the result. Above $Q^2 = 3.5$ GeV^2, only the NE11 experiment (solid circles in figure 1) has high precision data.

A recent experiment in Hall A [4] measured G_E/G_M by polarization transfer and found that G_E/G_M decreases with increasing Q^2 above $Q^2 = 1$ GeV^2, reaching a value of 0.6 at the highest Q^2 measured (see figure 2). This polarization transfer measurement is less prone to systematic issues than the L-T measurements and quotes significantly smaller uncertainties. The new results are clearly inconsistent with a constant value of $G_E/G_M = 1$, as favored by the global analysis of the L-T measurements. In fact, the Hall A results are consistent with only one of the four L-T measurements with data above $Q^2 = 2$ GeV^2. Additional data is being

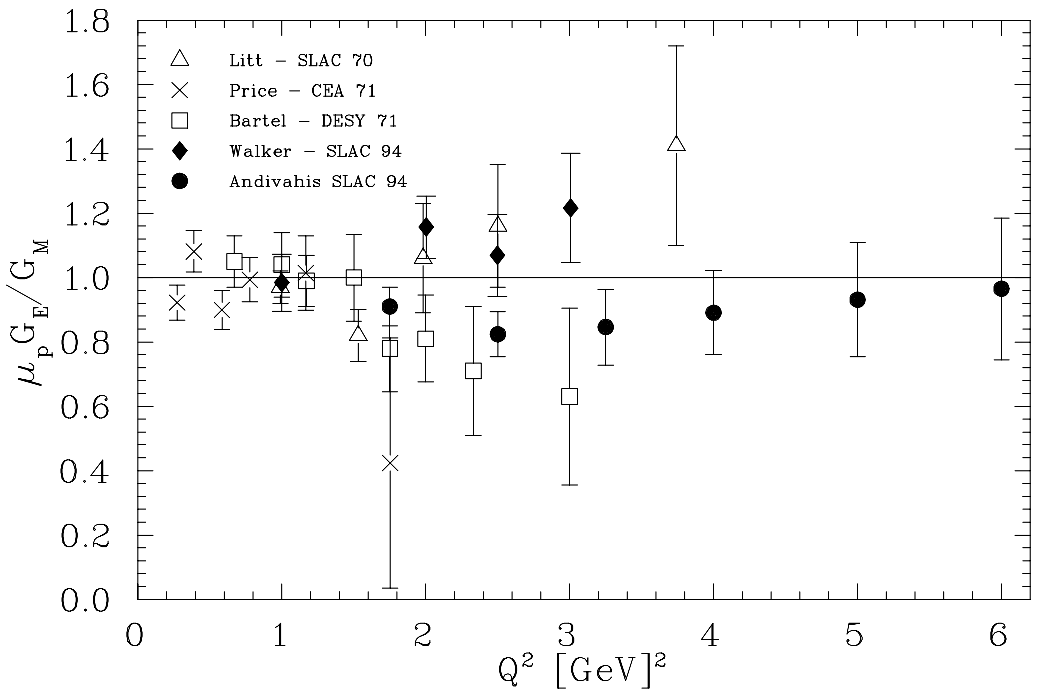

Figure 1: $\mu_p G_E/G_M$ as deduced from Rosenbluth separation measurements from SLAC, DESY, and CEA [1, 2].

taken in Hall A that will extend this measurement up to $Q^2 = 5.6$ GeV^2. The new Hall A results not only gives us a different picture for the Q^2-dependence of G_E/G_M, but also brings into question the SLAC L-T measurements. This impacts not only our understanding of the proton electric form factor, but may also impact other L-T measurements if there are a energy-dependent systematic uncertainties that have not been taken into account. An independent measurement of G_E/G_M in the region where we can achieve uncertainties comparable to or better than the Hall A measurement will be an important as a check on the value of G_E/G_M, and on the possibility of additional systematic uncertainties in the L-T or polarization transfer measurements. As the polarization transfer technique can be extended to large values of Q^2, where the L-T separation becomes increasingly difficult, it is important to have a precise comparison of the two techniques in the region where both can extract G_E/G_M with high precision.

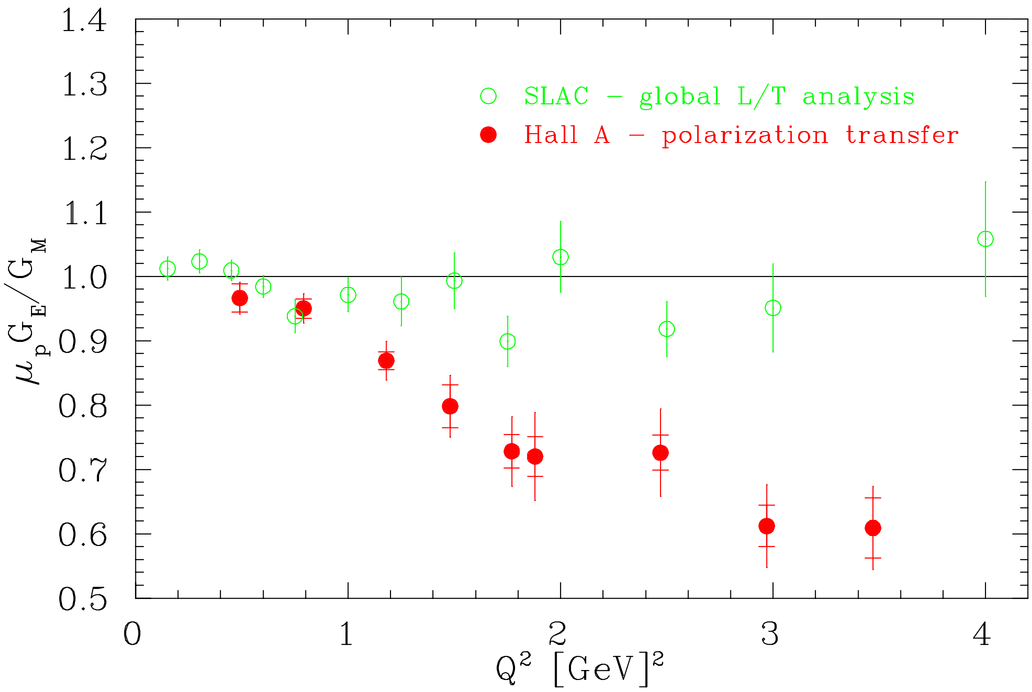

Figure 2: $\mu_p G_E/G_M$ as deduced from polarization transfer [4] (closed circles) and a global analysis of L-T separation measurements [1] (open circles).

We propose to measure G_E/G_M for the proton in a region where the previous determinations differ well outside of experimental uncertainties by utilizing the L-T separation technique in a new way in which only ratios of cross sections are used. Because of this the results are independent of target thickness and beam intensity and quite insensitive to uncertainties in beam energy. Protons rather than the usual electrons will be counted which reduces the variation with scattering angle, reduces the size of the radiative corrections and has the added advantage that the proton energy depends only on Q^2. Counting rates are high and a statistical accuracy of less than 0.3% can be achieved in less than a day of data taking at each point. We propose to take one-, two-, three-, and five- pass data with a fixed linac energy and in a total of 10 days determine G_E/G_M at $Q^2 = 1.45$ GeV^2 to $\pm$ 0.02, at 3.20 GeV^2

to ± 0.05 and at 4.90 GeV^2 to ± 0.10.

2 Method for Determining G_{E_p}/G_{M_p}

The differential cross section for e-p scattering can be written:

$$\sigma(E,\theta) = \sigma_0(E,\theta)(G_E^2 + \epsilon^{-1} G_M^2 Q^2 \kappa)$$

where E is the incident electron energy, θ the electron scattering angle, σ_0 the Mott scattering cross section, ϵ is the virtual photon polarization parameter, and $\kappa = (\frac{\mu_p}{2M_p})^2 = 2.212$. G_E and G_M are, of course, functions of Q^2 alone.

For a given E there is a one-to-one correspondence between θ and Q^2 and the cross section can be written:

$$\sigma(E,Q^2) = \sigma_0 G_M^2(\rho^2 + \epsilon^{-1} Q^2 \kappa)$$

where $\rho = \frac{G_E}{G_M}$.

For two energies, E$_A$ and E$_B$, at the same Q^2 the ratio of the cross sections is:

$$\frac{\sigma(E_A,Q^2)}{\sigma(E_B,Q^2)} = K \frac{\rho^2 + \epsilon_A^{-1} Q^2 \kappa}{\rho^2 + \epsilon_B^{-1} Q^2 \kappa}$$

where K is a kinematic factor.

If measurements at each energy are made simultaneously at two values of Q^2, Q_1^2 and Q_2^2, then there are two experimentally determined ratios:

$$R_A = \frac{\sigma(E_A,Q_1^2)}{\sigma(E_A,Q_2^2)} = K_A \frac{\rho_1^2 + \epsilon_{A1}^{-1} Q_1^2 \kappa}{\rho_2^2 + \epsilon_{A2}^{-1} Q_2^2 \kappa}$$

and

$$R_B = \frac{\sigma(E_B,Q_1^2)}{\sigma(E_B,Q_2^2)} = K_B \frac{\rho_1^2 + \epsilon_{B1}^{-1} Q_1^2 \kappa}{\rho_2^2 + \epsilon_{B2}^{-1} Q_2^2 \kappa}$$

and 2 ratios of physical interest, corresponding to the values of G_E/G_M at Q_1^2 and Q_2^2:

$$R_1 = \frac{\sigma(E_A, Q_1^2)}{\sigma(E_B, Q_1^2)} = K_1 \frac{\rho_1^2 + \epsilon_{A1}^{-1} Q_1^2 \kappa}{\rho_1^2 + \epsilon_{B1}^{-1} Q_1^2 \kappa}$$

and

$$R_2 = \frac{\sigma(E_A, Q_2^2)}{\sigma(E_B, Q_2^2)} = K_2 \frac{\rho_2^2 + \epsilon_{A2}^{-1} Q_2^2 \kappa}{\rho_2^2 + \epsilon_{B2}^{-1} Q_2^2 \kappa}$$

note that $\frac{R_A}{R_B} = \frac{R_1}{R_2}$, or $R_1 = R_2 \frac{R_A}{R_B}$.

The idea of the proposed measurements is to pick one value of Q^2 (Q_1^2) where the recently reported $\frac{G_E}{G_M}$ from the polarization transfer experiment [4] is very different from unity, and another Q^2 (Q_2^2) where $\frac{G_E}{G_M}$ must be close to its low-energy value of unity (with G_M in units of μ_p) and to pick kinematics such that ϵ_1 covers a wide range while ϵ_2 does not change a great deal. If, then, R_A and R_B are accurately measured and R_2 can be accurately calculated then R_1 is accurately determined. R_1 is a function of only ρ_1 ($=\frac{G_E}{G_M}(Q_1^2)$) and known quantities. We propose to do this at each of 3 values of Q_1^2, 1.45, 3.20 and 4.90 GeV^2, with a common Q_2^2, 0.5 GeV^2. These points are shown in Figure 3.

The proposed measurement is similar to the conventional Rosenbluth separation technique, but it has two major differences that give significant advantages. With one spectrometer, we perform a conventional Rosenbluth separation, but detect the protons, rather than the electrons. This gives a much larger range in ϵ by allowing us to measure at kinematics where the electron is at very small and very large angles. Detecting the proton leads to a reduced cross section dependence on the kinematics (beam energy and scattering angle) and reduces several systematic uncertainties when comparing the forward and backward angle measurements. While we make the primary measurement with one arm, we make a simultaneous measurement at low Q^2 where G_E/G_M is well known and where the ϵ range is very small. This will allow

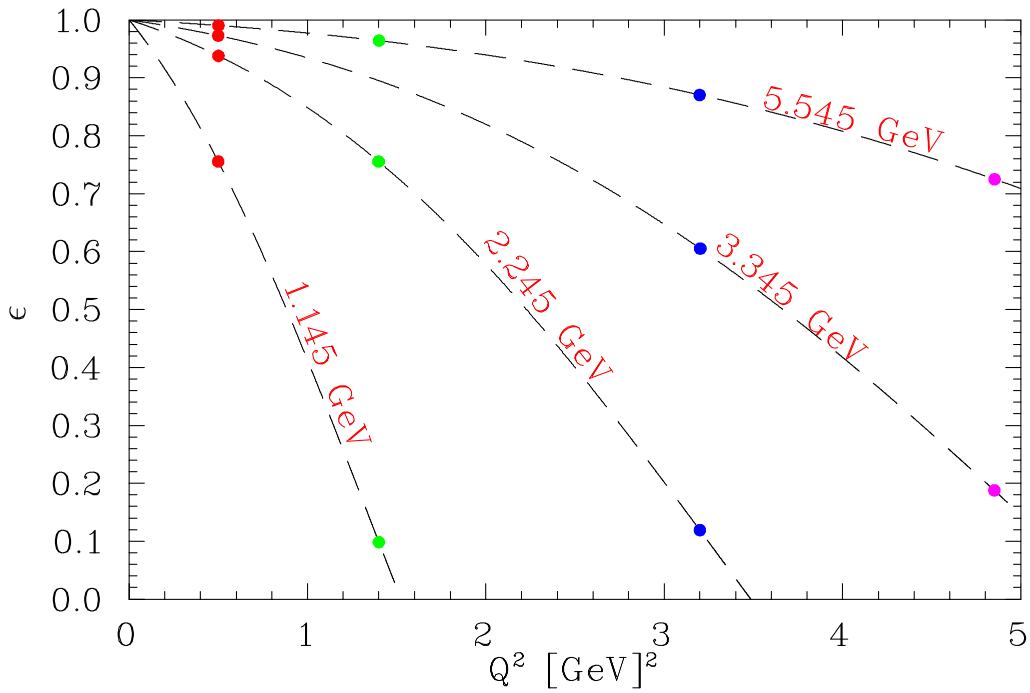

Figure 3: ϵ as a function of Q^2 at the proposed electron energies. The solid circles show the points at which data will be taken.

us to use the second arm as a luminosity monitor, removing the uncertainties due to beam charge and target density fluctuations. The major sources of uncertainty in the SLAC measurements [1] were uncertainty in the scattering kinematics, the total charge, and the target density. Because we measure the protons, we are less sensitive to knowledge of the scattering kinematics, and because we use the low Q^2 measurement as a luminosity monitor, we are insensitive to the measured charge and target thickness.

3 Experiment

3.1 Kinematics

The proposed kinematics are shown in table 1.

For this measurement, proton detection has several advantages over electron detection. Protons at moderately large angles correspond to forward angle electrons. Detecting the proton allows us to go to lower values of electron scattering angle, down to $\sim 7^\circ$ for this proposal, than would normally be possible. It also reduces the effect of uncertainty in the measured scattering angle. The cross section for forward angle electrons varies rapidly with scattering angle, while the cross section dependence for the corresponding protons is smaller by a factor of 2-3 for the kinematics where this is a dominant source of uncertainty (as seen in Table 1). The reverse is true for the backwards angle electrons: the angular variation of the cross section is greater for the protons. However, it is a much smaller effect than for the forwards angle electrons, and therefore the increased kinematical dependence does not increase the overall uncertainty in the extracted form factors. The limitation for backwards angle electrons is the reduced cross section within the angular acceptance of the spectrometer. Again, measuring the proton leads to a significant improvement, as the forward angle protons are in a narrow angular range compared to the corresponding backwards angle electrons. Finally, detection of the proton reduces the cross section variation with beam energy for all kinematics.

In addition to the kinematic advantages of detecting the proton, the systematic uncertainties in the Rosenbluth separation are smaller when the proton is measured. This is due to the fact that the proton momentum is the same for all ϵ values at a given Q^2. Thus the magnets are not set to different currents when ϵ is changed (which could lead to small modifications to the optics), and momentum dependence corrections such as detector efficiency and multiple scattering will be nearly identical

Proton kinematics								
E_e (GeV)	Q^2 (GeV)^2	ϵ	θ_p (deg)	Proton K.E.(GeV)	Proton Momentum	σ_p^{SLAC} (cm^2/msr)	$\Delta\sigma$ %/deg	$\Delta\sigma$ %/(%E_e)
1.162	0.50	.762	50.407	0.266	0.756	4.540e-32	13.26	4.22
1.162	1.45	.081	12.540	0.773	1.431	1.640e-33	3.65	4.00
2.262	0.50	.939	60.075	0.266	0.756	6.373e-32	18.56	4.67
2.262	1.45	.746	40.175	0.773	1.431	2.334e-33	14.68	5.36
2.262	3.20	.131	12.525	1.705	2.471	1.227e-34	5.51	4.43
3.362	0.50	.973	63.191	0.266	0.756	7.238e-32	20.93	4.83
3.362	3.20	.610	28.048	1.705	2.471	1.429e-34	14.08	5.48
3.362	4.90	.181	12.664	2.611	3.423	2.617e-35	7.34	4.58
5.562	0.50	.990	65.664	0.266	0.756	8.050e-32	23.16	4.97
5.562	1.45	.963	50.864	0.773	1.431	3.227e-33	20.71	6.13
5.562	3.20	.871	36.255	1.705	2.471	1.751e-34	19.17	6.30
5.562	4.90	.722	26.942	2.611	3.423	3.143e-35	17.48	5.91
Electron kinematics								
E_e (GeV)	Q^2 (GeV)^2	ϵ	θ_e (deg)	Electron K.E.(GeV)	σ_e^{HallA} $/\sigma_e^{SLAC}$	σ_e^{SLAC} (cm^2/msr)	$\Delta\sigma$ %/deg	$\Delta\sigma$ %/(%E_e)
1.162	0.50	.762	40.557	0.896	0.973	4.064e-32	14.70	8.69
1.162	1.45	.081	127.062	0.389	0.991	1.185e-34	2.40	10.07
2.262	0.50	.939	19.158	1.996	0.969	2.217e-31	33.19	8.98
2.262	1.45	.746	38.299	1.489	0.934	1.933e-33	18.20	11.77
2.262	3.20	.131	105.695	0.557	0.988	6.077e-36	3.62	11.49
3.362	0.50	.973	12.584	3.096	0.969	5.479e-31	51.20	9.05
3.362	3.20	.610	44.541	1.657	0.949	5.667e-35	15.20	13.06
3.362	4.90	.181	88.315	0.751	0.987*	1.228e-36	4.92	12.08
5.562	0.50	.990	7.470	5.296	0.969	1.629e-30	87.01	9.09
5.562	1.45	.963	13.398	4.789	0.919	2.282e-32	59.89	12.59
5.562	3.20	.871	22.269	3.857	0.930	3.438e-34	37.05	14.24
5.562	4.90	.722	31.710	2.951	0.950*	1.751e-35	23.69	14.20
					*assumes $G_E/G_M = 0.45$ at $Q^2 = 4.90$			

Table 1: Proton kinematics for the proposed measurement. The corresponding electron kinematics are included for comparison.

for the forwards and backwards angle measurements. While there will be small angle-dependent differences in multiple scattering due to the target geometry, the proton momentum will be identical, making the differences smaller than the would be if the electron were detected. The effect of any rate dependent efficiencies on the separation will also be reduced because the difference in cross sections between forward and backwards angles is much smaller than in the case where the electron is detected. Finally, because the scattered electron is not detected, the radiative corrections are significantly smaller (on average by a factor of two).

There will be corrections to the absolute cross section that are larger for measured protons, but for the most part these cancel in the ratios. Proton absorption in the target and spectrometer leads to a correction of a few percent. However, the absorption in the spectrometer will completely cancel when comparing the different ϵ values, as the proton momentum is identical at all kinematics. There will be a difference absorption in the target because the amount of target material seen by the outgoing proton depends on the scattering angle. For the standard 'beer can' target (4cm length, 6.35cm diameter), the path length through the target varies between 2cm and 3.76cm, which gives a maximum difference of 0.26% in the proton absorption. This will be even smaller if improved target cells (with a smaller diameter) or 'tuna can' cells are used. The target geometry is taken into account in the simulation, and this small difference in absorption can be taken into account in the analysis, with a negligible uncertainty in the final result.

Protons are not always stopped by the HRS collimator, so one can not rely on the collimator to define the solid angle for the measurement. We will define the solid angle using cuts on the reconstructed scattering angles, in a region where the HRS has nearly complete acceptance. While any error in the angular reconstruction will lead to an uncertainty in the absolute solid angle, identical cuts will be used at forwards and backwards angle, and so much of the uncertainty in the solid angle will cancel. As the spectrometer angle changes, the length of the target as seen by the HRS also changes. Thus, any target position dependence of the reconstruction can lead to a change in solid angle. We will measure this position dependence with sieve slit and elastic runs on a 15cm target and the variable z-position optics targets, and use this to correct for target length variation with scattering angle. The high Q^2 data is taken at smaller scattering angles, where the target length dependence should not be a large problem. The $Q^2 = 0.5$ GeV^2 normalization points are taken at larger angles but the angle difference between the high and low ϵ points are small. The change in target length as seen by the HRS is <20% for the $Q^2 = 1.45$ point, and $\lesssim$5% for the other kinematics). The $Q^2 = 1.45$ GeV^2 point does have a large change in scattering angle (from 12.5° to 51°), and we will have to rely on measurement of the solid angle dependence to determine the size of the correction. While we will have to measure the position dependence before we know the size of the correction (and uncertainty), we will assume an additional uncertainty of 0.5% to the acceptance for the $Q^2 = 1.45$ GeV^2 point to take into account the larger potential solid angle variation. Once we have measured the solid angle dependence on target position, we may well be able to correct to better than 0.5%, but we would like to note that even if the uncertainty turns out to be twice as large, the uncertainty on the extracted value of G_E/G_M at this Q^2 is still ± 0.03, smaller than the uncertainty in the polarization transfer measurement, and 6 standard deviations from unity if the Hall A result is correct.

3.2 Backgrounds

The biggest problem with detecting the protons is the presence of background processes that generate protons close to the elastic peak. In particular, photoproduction of neutral pions will cause a background of high energy protons. For the low Q^2 data, the threshold for pion production is far enough below the elastic peak that it can be easily cut away. For the higher Q^2 value, these protons can have momenta less than 1% below the elastic peak. For these kinematics, we will need to subtract away these contributions. Figure 4 shows a measured spectrum of proton elastic singles from a Hall A measurement at $Q^2 = 3.0$ GeV^2, along with a monte carlo simulation of the contributions from elastic scattering from protons (smeared to match the HRS resolution), quasielastic scattering from the aluminum target windows, and protons coming from pion photoproduction (using $\mathrm{d}\sigma/\mathrm{d}t \propto s^{-7}$, and normalizing to the measured distribution). For a cut of $|\delta p/p| < 1\%$, the pion photoproduction background is a 3% contribution to the yield, and is well reproduced by the calculated photoproduction spectrum.

While the calculated elastic spectrum plus pion photoproduction background does a good job of reproducing the proton spectrum, we will make additional tests of our photoproduction background calculation. For roughly half of the kinematics, the pion photoproduction threshold is well separated from the elastic peak, and we can test our photoproduction spectrum with only the tail of the elastic peak as background. We will have coincidence runs at three kinematics, which will allow us to separate the elastic and the photoproduction in order to test our calculations of the lineshapes. As an additional test we will put a hodoscope in the hall to tag electrons corresponding to the detected elastic protons for all forward angle kinematics (where the electrons are scattered at larger angles). By rejecting events where an electron is detected, we can examine inclusive protons with the elastic peak suppressed in order to compare the photoproduction background to our calculated lineshape. By rejecting events with no detected electron, we can generate a sample of events with a suppressed photoproduction background. We will not use the electron hodoscope to remove background events in the analysis, because it would reject events due to radiation of the outgoing electron and because any difference in efficiency or solid angle matching between the high and low ϵ points could introduce a large uncertainty in the result.

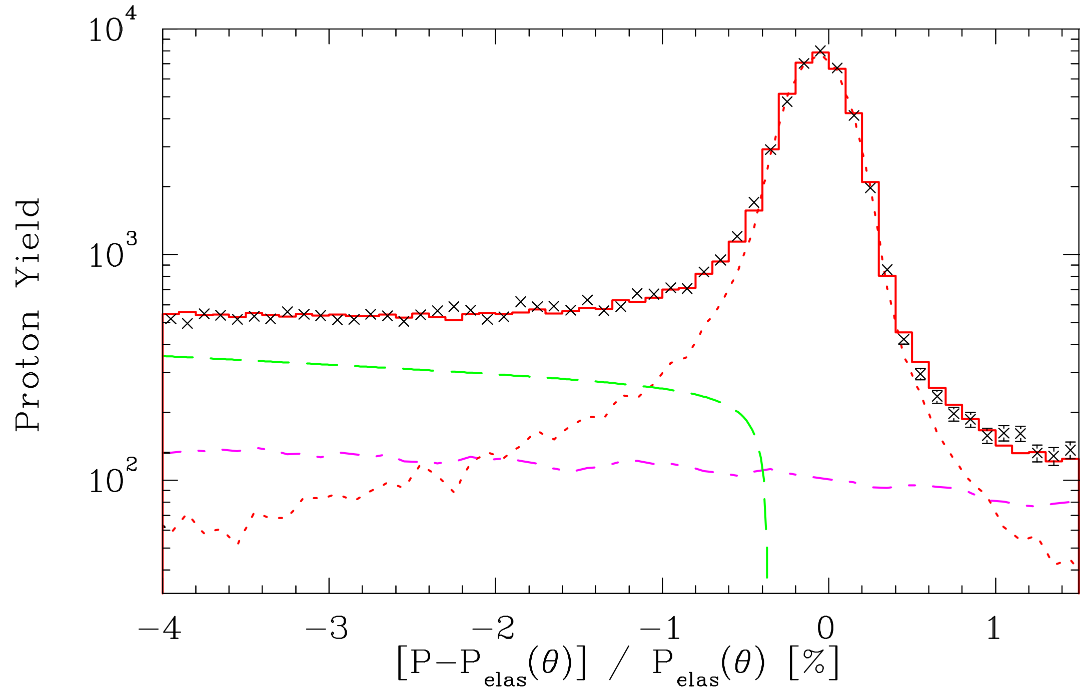

Figure 4: HRS Proton elastic singles spectrum for E_0 = 3.4 GeV, Q^2 = 3.0 GeV^2 (crosses). The curves show simulations of the elastic scattering (dotted), endcap contributions (dash-dot), and pion photoproduction (dashed), and the histogram shows the sum of the simulated contributions.

There will also be a background of charged pion photoproduction. For several kinematics (including most of the high Q^2 kinematics), the pion production threshold is far enough below the elastic peak to cleanly separate the pions. For the other kinematics, time of flight will efficiently remove pions for the low Q^2 data, and an Aerogel detector will be used to reject pions where the time of flight is not fully efficient. In addition, having both Aerogel and time of flight separation will allow us to determine the efficiency of the particle identification cuts.

3.3 Spectrometers

The experiment is proposed for Hall A using the two spectrometers and the cryogenic target. The 4 cm liquid H_2 target would be viewed at the maximum angle of 65 degrees and the angle only changes by a total of 15 degrees for the low Q^2 point. An Aerogel detector will be used for p/π separation. Solid angles would be restricted to about 1.6 msr by software cuts. At each angular setting the spectrometers will be surveyed and also data taken with a carbon target whose position can be very accurately set in order to verify the pointing of the spectrometer.

3.4 Yields

A beam of 50 μA on a 4 cm liquid hydrogen target gives a luminosity of 5.4×10^{37} which with a 1.6 msr solid angle means that the expected yields can be obtained by multiplying the cross sections in Table 1 by 8.6×10^{34}. This would mean 2.4 counts/second or about 8600 counts/hour at the lowest yield point, $E_e = 3.362$ GeV, $\theta_p = 12.664^o$ and about 2.8 counts/second at the other $Q^2 = 4.90$ GeV^2 point. The cross sections are a factor of 4 or more higher at all of the other settings.

3.5 Systematic Uncertainties

Because of the high precision required for this measurement, we have to insure that we take into account many small corrections that are often ignored. Dead time corrections, bin centering, and uncertainties in the kinematic quantities all have to be corrected precisely.

Computer dead time corrections are measured in the standard data acquisition system in Hall A. The number of triggers generated and the number of events actually written to tape are recorded, and the cross section is corrected by the fraction of events sampled, with a very small associated uncertainty. Electronic dead time cannot be measured in the same direct way. For our experiment, we estimate the total trigger rate of the hodoscopes to stay below 200-300kHz. The current electronics use gate widths of $\sim$200 ns, which would lead to dead times of up to 4-6%. Recent modifications to the electronics allow a measurement of the electronic dead time throughout the run. In addition, there is a plan to change the electronics so that the trigger signals will use 40 ns gate widths, which will reduce the maximum electronic dead time to $\sim$1%, and the typical uncertainty on this correction should be $<$0.1%.

Our estimates assume that we will accept protons over a $\pm$10mr angular range in scattering angle. Because the cross section is not constant over this range, we will need to apply a bin centering correction to extract the cross section at the central scattering angle. The cross sections can vary significantly over the measured range, but the bin centering correction is quite small because over the 20mr acceptance, the cross section is nearly linear and the acceptance is flat. Simulations of elastic scattering at each of the kinematics including both the cross section variation and geometric acceptance show no significant bin centering corrections, and indicate that the uncertainty in the bin centering correction is $<$0.1%.

The largest systematic uncertainties come from uncertainty in the scattering kinematics. For a beam energy uncertainty of 0.1%, the cross sections vary by about 0.5%. However, the high and the low Q^2 measurements at each beam energy have a similar energy dependence (table 1), and so the effect of a 0.1% energy uncertainty is only $\sim$0.1% in the final measured ratio. In addition, if the errors at different energies are correlated (*i.e.* if linac scaling holds), then there will be additional cancellation between the forwards and backwards measurements. Uncertainty in the scattering angle will have a larger effect on the extracted ratio. There are two contributors to the scattering angle uncertainty: The incoming beam angle, and the scattered proton angle. There are two BPMs just upstream of the the target.

They can be surveyed (relative to the nominal beamline) to within 0.5mm, and are separated by 6 meters, giving an uncertainty in the beam angle of 0.12mr. However, the change in angle from run to run (measured with the BPM) can be measured much more accurately, so the 0.12mr offset will be the same for both the forwards and backwards angle runs at each Q^2 point, and the effect of the angle offset will partially cancel between the high and low epsilon points. Because of this, the 0.12mr offset corresponds to an uncertainty in the final ratio of $<0.2\%$.

The uncertainty in the angle of the scattered proton also breaks down into an overall offset (identical for both forward and backwards angles) and an offset that can vary randomly as the spectrometer angle is changed. The overall offset comes from offsets in the VDC positions relative to the optical axis and from errors in the scattering angle reconstruction. Because we will define the scattering angle acceptance with software cuts rather than with a collimator, an error in the angle reconstruction will modify the size and central angle for the defined angular acceptance. We will use the same cuts for all data and so the uncertainty in the total solid angle will largely cancel, but there can still be an overall offset in the central scattering angle of the software restricted window. Offsets that vary randomly with changing scattering angle come from any shifts of the VDC position during the run, as well as uncertainty in the pointing of the spectrometer. As we will survey the HRS pointing at each setting, the pointing uncertainty will be relatively small. While the survey gives the mechanical axis (as determined by the magnet positions) rather than the true optical axis, the difference is the same at all angles, and is taken as part of the constant offset in the angle reconstruction uncertainty. We estimate a random uncertainty of 0.13mr, and a constant offset uncertainty of 0.20mr. A 0.20mr offset gives an uncertainty in the extracted ratios of $\sim$0.2%, while an 0.13mr random uncertainty contributes $\sim$0.24% to the uncertainty.

Our total uncertainty in the scattering angle (combining the fixed offsets, random offsets, and beam angle offsets) is 0.27mr. This is slightly smaller than the quoted uncertainties used by previous Hall A measurements, but is consistent with the assumptions used. The typical scattering angle uncertainty used in the analysis of the completed Hall A analyses has been 0.3-1.0mr (usually 0.3-0.5mr). Experiments that have done complete surveys of the spectrometer pointing and used kinematic checks of the angle have routinely achieved 0.3mr uncertainty, but we have an additional advantage in that we do not limit the solid angle with the collimator. As it is located $\sim$1 meter from the target, even a small offset of the collimator from the optical axis will offset the central angle of the acceptance. If survey or data can determine its position to 0.1-0.2mm, this is still a 0.10-0.20mr contribution to the uncertainty in the scattering angle, in addition to the uncertainty coming from the spectrometer pointing and incoming beam angle. Because we use software cuts to define the scattering angle acceptance, uncertainties in the central angle come from the HRS pointing and uncertainties in the VDC position, which have a much smaller effect than a comparable uncertainty in the collimator position. With careful surveys at each point, monitoring of the HRS pointing with the LVDTs (linear voltage differential transformers), and several kinematic checks on the spectrometer angle (as discussed in the run plan), we should be able to achieve the assumed angular uncertainty. Table 2 shows the projected uncertainty for the measurement at each value of Q^2.

3.6 Run Plan

Table 3 shows the proposed run plan for the experiment. We will take data in both spectrometers simultaneously for all kinematics. Data will be taken on 4cm LH_2 and aluminum 'dummy' targets for endcap subtraction. An arc energy measurement and e-p energy measurement will be done at each beam energy, and the spectrometer will be surveyed before (or after) each data taking run. The checkout runs will include

Source	Size	δR1/R1 ($Q^2 = 1.45$)	δR1/R1 ($Q^2 = 3.20$)	δR1/R1 ($Q^2 = 4.90$)
Statistics	0.1-0.3%	0.32%	0.39%	0.45%
Beam Energy	0.05%	0.06%	0.04%	0.05%
Beam Angle	0.12 mr	0.18%	0.13%	0.11%
θ_p(random)	0.13 mr	0.22%	0.27%	0.27%
θ_p(fixed offset)	0.20 mr	0.22%	0.17%	0.12%
Bin Centering		0.06%	0.06%	0.06%
Dead Time		0.10%	0.10%	0.10%
Dummy Subtraction	0.1%	0.20%	0.20%	0.20%
Radiative Corrections	2.5%	0.22%	0.34%	0.28%
$Q^2 = 0.5$ G_E/G_M value	2.0%	0.27%	0.05%	0.02%
*Acceptance	0.1%	0.50%	0.20%	0.20%
*Efficiency	0.1%	0.20%	0.20%	0.20%
*Luminosity	0.1%	0.20%	0.20%	0.20%
Total		0.86%	0.75%	0.75%
Error on G_E/G_M		2.1%	3.9%	8.2%

Table 2: Projected uncertainties for the proposed measurement. These estimates conservatively allow for a 0.1% random fluctuation for those corrections which we expect will entirely cancel between the forwards and backwards angle (those marked with '*'). The error on the extracted G_E/G_M depends on the value of G_E/G_M. The quoted values assume $G_E/G_M = 1.0$ at all Q^2 values.

sieve slit runs with electron singles and elastic coincidences, and sieve slit runs with a long (15cm) target and with the variable z-position optics target to measure any correlation between target position and reconstructed scattering angle.

In addition to the proton inclusive data for the G_E/G_M measurement, we will take several test measurements. Runs will be taken at different beam currents in order to verify our measurement of the dead time in the spectrometers. Data will be taken with a thin carbon target at all kinematics as a check on the spectrometer pointing. Finally, because we define the kinematics by the proton angle, we can use the measured proton momentum as a check on the kinematics. While for a single setting, it is not possible to disentangle a momentum offset from a scattering angle offset, the magnets settings stay the same when the scattering angle is changed, and so any momentum offset will be identical at all epsilon points for a given Q^2. The reproducibility of the magnet settings, important if one of the magnet trips and has to be reset, is $\sim 10^{-4}$, small enough that it is not a significant problem for kinematics checks. This will allow us to use the reconstructed momentum as an additional check on the kinematics.

Finally, coincidence data will be taken at some energies as a check of the scattering kinematics, and as a measure of proton detection efficiency and absorption (though these corrections almost completely cancel in the extracted ratios). For $Q^2 = 1.45$ GeV^2, we will take singles and coincidence data at coincidence kinematics at 1, 2, and 3 passes. Comparing the elastic cross section as measured by the protons and the electrons at one kinematics allows us to measure the proton inefficiency (due mainly to absorption). By comparing electron singles to proton singles at multiple kinematics (with a fixed proton momentum), we can also check the radiative corrections, which are significantly different for electron and proton singles.

Checkout, calibration, and sieve runs at 1.16 GeV.	20 hours	
Singles and coincidence H_2 data at 3 beam currents.	3+1 hours	24 hours
Move spectrometers to coincidence $Q^2 = 1.45$ and survey.	6 hours	
Coincidence run at $Q^2 = 1.45$.	2+1 hours	
Move electron spectrometer to proton $Q^2 = 0.5$ and survey.	6 hours	
Data run at $Q^2 = 0.5$ and 1.45.	1+1 hours	
Change energy to 2.26 GeV and move spectrometers.	8 hours	
Data run at $Q^2 = 0.5$ and 1.45.	2+1 hours	
Survey spectrometers.	6 hours	
Move spectrometers to coincidence $Q^2 = 1.45$ and survey.	6 hours	
Coincidence run at $Q^2 = 1.45$	4+2 hours	
Change energy to 5.56 GeV and move spectrometers.	8 hours	
Data run at $Q^2 = 0.5$ and 1.45.	1+1 hours	
Survey spectrometers.	6 hours	62 hours
Move spectrometers to $Q^2 = 0.5$ and 3.20 and survey.	6 hours	
Data run at $Q^2 = 0.5$ and 3.20.	10+3 hours	
Change energy to 2.26 GeV and move spectrometers.	8 hours	
Data run at $Q^2 = 0.5$ and 3.20.	8+2 hours	
Survey spectrometers.	6 hours	
Change energy to 3.36 GeV and move spectrometers.	8 hours	
Data run at $Q^2 = 0.5$ and 3.20.	12+3 hours	
Survey spectrometers.	6 hours	
Move spectrometers to coincidence $Q^2 = 1.45$ and survey.	6 hours	
Coincidence run at $Q^2 = 1.45$.	4+2 hours	84 hours
Move spectrometers to $Q^2 = 0.5$ and 4.90 and survey.	6 hours	
Data run at $Q^2 = 0.5$ and 4.90.	20+5 hours	
Change energy to 5.56 GeV and move spectrometers.	8 hours	
Data run at $Q^2 = 0.5$ and 4.90.	20+5 hours	
Survey spectrometers.	6 hours	70 hours
Total		240 hours

Table 3: Run plan for the proposed measurement. Where two times are listed (*e.g.* 10+3 hours), the first time listed is for hydrogen runs, and the second is for carbon and dummy runs.

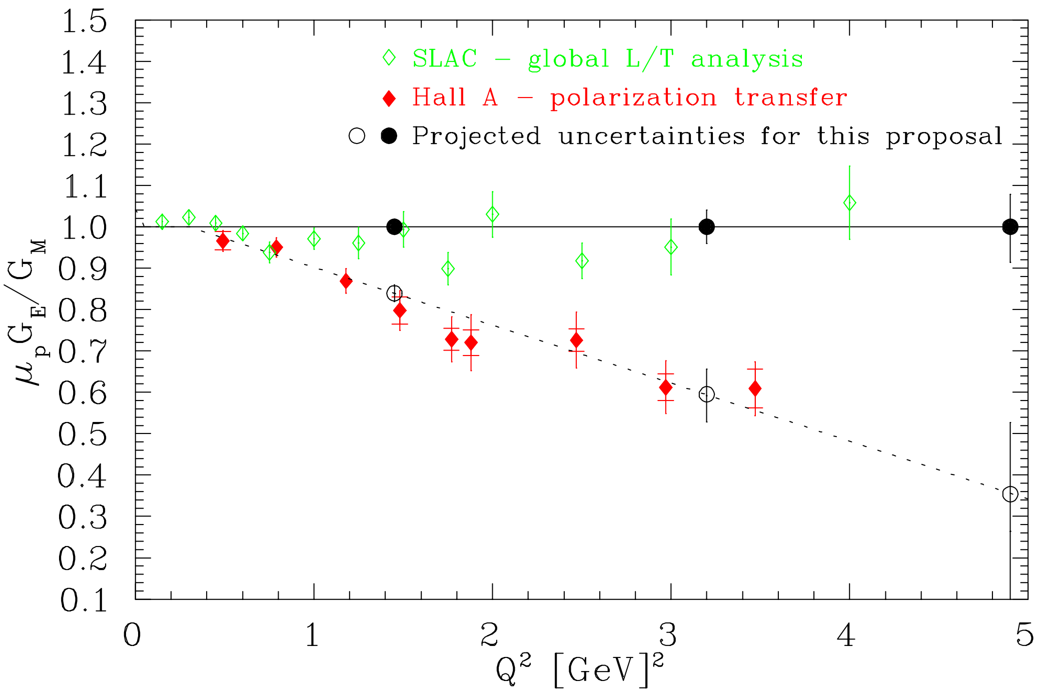

Figure 5: $\mu_p G_E/G_M$ as deduced from polarization transfer [4] (closed diamonds) and a global analysis of L-T separation experiments [1] (open diamonds). The circles show the projected uncertainties for the proposed measurement for two different assumptions. The closed circles assume $\mu_p G_E/G_M = 1$ and the open circles are based on a fit to the Hall A data (dashed line).

4 Conclusions

With 10 days of running time spread over 4 energies, ratios which depend only on G_E/G_M of the proton can be measured to ~0.75% at three values of Q^2. We will take data at values of Q^2 where Hall A polarization transfer experiment [4] finds G_E/G_M to be significantly less then unity. At the two lower Q^2 points which overlap the published polarization transfer results the difference between the assumption of $G_E/G_M = 1$ and the reported polarization transfer leads to a 7% difference in the ratio we will measure, almost ten times our expected uncertainty. Figure 5 shows the projected uncertainties on the extracted value of G_E/G_M, under two different assumptions for the value of G_E/G_M. The projected uncertainties are significantly smaller than from previous L-T measurements, while for the $Q^2 =$ 1.45 and 3.20 GeV^2 points, where published polarization transfer data exists, the projected uncertainty is comparable to or smaller then the Hall A measurement. At $Q^2 = 4.9$, the uncertainty on G_E/G_M is starting to become large, but the value as taken from the fit to the Hall A data is still almost 6 standard deviations from unity.

References

[1] R. C. Walker *et. al.* Phys. Rev. **D49** 5671 (1994).

[2] L. Andivahis *et. al.* Phys. Rev. **D50**, 5491 (1994); A. F. Sill *et. al.* Phys. Rev. **D48**, 29 (1993); W. Bartel *et. al.* Nucl. Phys. **B58**, 429 (1973); L. E. Price *et. al.* Phys. Rev. **D4**, 45 (1971); J. Litt *et. al.* Phys. Lett. **31B**, 40 (1970)

[3] P. E. Bosted, Phys. Rev. **C51** 409 (1994).

[4] M. K. Jones *et. al.* Phys. Rev. Lett, **84**, 1398 (2000).